Performance Analysis of Relay Selection on Cooperative Uplink NOMA Network with Wireless Power Transfer

Van-Long Nguyen[1(✉)], Van-Truong Truong[2], Dac-Binh Ha[2,3], Tan-Loc Vo[4], and Yoonill Lee[5]

[1] Graduate School, Duy Tan University, Danang 550000, Vietnam
vanlong.itqn@gmail.com
[2] Faculty of Electrical-Electronic Engineering, Duy Tan University, Danang 550000, Vietnam
truongvantruong@dtu.edu.vn, hadacbinh@duytan.edu.vn
[3] Institute of Research and Development, Duy Tan University, Danang 550000, Vietnam
[4] Pham Van Dong University, Quang Ngai, Vietnam
vtlocqng@gmail.com
[5] Department of Engineering Technology, Purdue University Northwest, Hammond, IN, USA
lee2273@pnw.edu

Abstract. Wireless power transmission in the next-generation wireless networks is the subject that attracts a lot of attention from academia and industry. In this work, we study and analyze the performance of relay selection on uplink non-orthogonal multiple access (NOMA) networks with wireless power transmission. Specifically, the considered system consists of one base station, multiple power-constrained relays and a pair of NOMA users. The best relay (with highest energy harvested from the base station) is chosen to cooperate with two users which use NOMA scheme to send messages to the base station. To analyze the performance, based on the statistical characteristics of signal-to-noise ratio (SNR) and signal-to-interference-plus-noise ratio (SINR), using the Gaussian-Chebyshev quadrature method, the closed-form expressions of outage probability and throughput for two users are derived. In order to understand more details about the behavior of this considered system, the numerical results on outage probability and throughput of a given system are provided following the system key parameters, such as the transmit power, the number of relays, time switching ratio and energy conversion efficiency. In the end, the theoretical result is also verified by using the Monte-Carlo simulation. The simulation results demonstrate that the performance of the system is improved by increasing the number of relays.

Keywords: Non-orthogonal multiple access · Wireless power transfer · Cooperative network · RF energy harvesting · Outage probability · Throughput

N.-S. Vo and V.-P. Hoang (Eds.): INISCOM 2020, LNICST 334, pp. 32–44, 2020.
https://doi.org/10.1007/978-3-030-63083-6_3

1 Introduction

In recent years, we have witnessed an explosion in the number of wireless devices: smartphones, wireless sensors, wireless devices, etc. These devices are increasingly integrated with many functions, leading to the urgent need for the power supply. One of the methods that attracted the attention of both academics and the industry is radio frequency (RF) energy harvesting (EH), which enables the converting of the received RF signals into electricity energy [1–5]. We also realize that the growingtrend of wireless networks is to serve a greater number of users while still have faster data transmission speed and higher reliability. In recent years, there has been many researches on 5G networks to reach that goal, in which, NOMA has emerged as the strongest candidate with the ability to serve multiple users using the same amount of time and frequency resources [6–8]. Most of articles currently focus on NOMA downlink networks [9,10], while uplink networks [11–14] are equally important in many systems, such as wireless sensors networks. The paper [11] proposed uplink NOMA network for two users, in which, users with better channel condition communicated directly with Base Station (BS), while the remaining user with bad channel condition was supported by half-duplex decode-and-forward (DF) relay. The uplink NOMA model in which the cell-center user directly connected to the BS and DF relay, while the cell-edge user communicated with the BS with the help of DF relay, is proposed in [12]. The outage probability and average sum rate were analyzed to study the performance of this considered system. The [13] studied NOMA uplink system with massive connectivity requirements, including Internet of Things (IoT) nodes, mobile devices, or unmanned aerial vehicles (UAVs). In particular, users can select buffer-aided (BA) relay in the cluster of relays, which is called flex-NOMA, to minimize packet delay. Outage probability of system is presented for comparing with OMA model. Another study of two-user uplink NOMA is presented in [14], in which, user near the BS acts as a transducer which can be switched in half-duplex or full-duplex to aid communication between remote users with BS. Two scenarios are given by the author to evaluate the system: (1) a direct channel between the BS and remote users and (2) no direct channel between BS and remote users.

As such, the combination between NOMA and relay techniques and RF EH will be considered for the new generation network.

Different from the works above, our work focus on the performance analysis of relay selection on cooperative uplink NOMA network with wireless power transfer. Our article contributes to the ideas below:

1. Proposing the relay selection on cooperative uplink NOMA network with wireless power transfer scheme.
2. Deriving exact closed-form expressions of outage probability and throughput for each user.
3. Evaluating the performance using tools of outage probability and throughput expressions.
4. The behavior of the considered system is assessed concerning different key parameters, such as transmit power, number of the relay, time switching ratio and energy conversion efficiency.

The rest of this paper is organized as follows. The system model is presented in Sect. 2. The performance of the considered system is analyzed in Sect. 3. The numerical results are shown in Sect. 4. Finally, Sect. 5 draws the conclusion of our paper.

2 Network and Channel Models

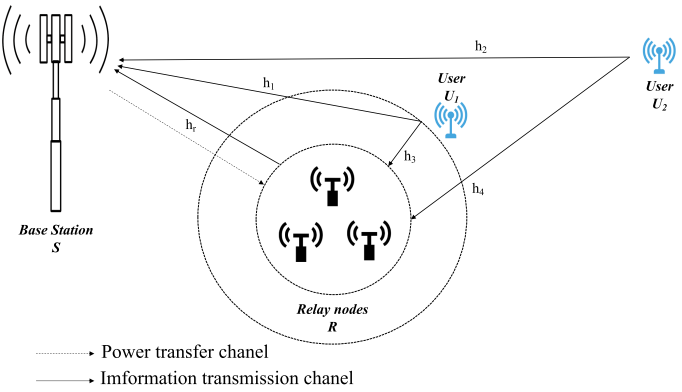

Fig. 1. System model for uplink NOMA AF relaying network

Figure 1 is a model of an uplink cooperative NOMA system in which the signals are transmitted from the two NOMA users (near user U_1 and far user U_2) to the base station (S) with the cooperation of energy-constrained amplify-and-forward relay nodes (R). Assuming that all users and relay nodes are single antenna devices and operate in half-duplex mode. The relay nodes are located closer to the base station than the users. With two users, the one that has shorter distance to the base station is named as U_1, the farther one is U_2.

At the beginning of each transmission, the channel information from S to the relays is collected by the base station using pilot signals. Thereby, S identifies the relay with the best ability to receive energy to specify it the relay node from the user to the base station. The protocol for this system is proposed as follows:

1. In the first phase (Power transfer phase): Based on Rayleigh fading channel coefficient from link S to relay nodes R (h_r), S chose the relay node (R^*), which had the best Rayleigh fading channel coefficient (h_{r^*}) to transmit RF energy with power P_0 in the time αT where $\alpha (0 < \alpha < 1)$ denotes the time switching ratio and T is the block time.
2. In the second phase (Information transmission phase): Users U_1 and U_2 simultaneously broadcast their signals (s_1, s_2) to S and R on the same frequency blocks, following the NOMA scheme within the duration of $(1 - \alpha)T/2$.

3. In the third phase (Relay phase): R^* amplifies the received signal and forwards to S in the remaining time of $(1-\alpha)T/2$ with the energy harvested from S by using the best Rayleigh fading channel coefficient (h_{r^*}).

Finally, S uses the selection combining (SC) scheme and successive interference cancellation (SIC) to combines two received signals, i.e., the direct signal from users and the relaying signal from R^* [15].

2.1 Power Transfer Phase

In this phase, S transmits energy to the relay nodes with a power of P_0, the energy gained at the relay during αT can be described as follow:

$$E_{R^*} = \frac{\eta P_0 |h_{r^*}|^2 \alpha T}{d_{r^*}^{\theta}}, \tag{1}$$

where η indicates the energy conversion efficiency ($0 < \eta < 1$), $|h_r^*|^2$ denotes the Rayleigh fading channel coefficient of $S - R^*$, d_{r^*} is the Euclidean distance of link $S - R^*$ and θ is denoted as the path-loss exponent.

2.2 Information Transmission Phase

In the second phase, both users U_1 and U_2 simultaneously broadcast their own information to base station and relays in the duration of $(1-\alpha)T/2$. It is assumed S applying SIC to decode s_1 and s_2 from the direct signal. The instantaneous SINR for detecting the signal from U_1 is:

$$\gamma_d^{s_1} = \frac{P_1 |h_1|^2 / d_1^{\theta}}{P_2 |h_2|^2 / d_2^{\theta} + \sigma^2} = \frac{\gamma_1 |h_1|^2}{\gamma_2 |h_2|^2 + 1} \tag{2}$$

The SNR for detecting the signal from U_2 is:

$$\gamma_d^{s_2} = \gamma_2 |h_2|^2 \tag{3}$$

where $\gamma_1 = \frac{P_1}{\sigma^2 d_1^{\theta}}, \gamma_2 = \frac{P_2}{\sigma^2 d_2^{\theta}}$ are denoted as SNR at U_1 and U_2, P_i ($i = \{1, 2\}$) denote the transmit powers of users U_1 and U_2, respectively. h_i denotes Rayleigh fading channel coefficients between users and S. Note that in this paper, the received signal at S and R^* are y_1 and y_2, respectively, similar to the formulas (2) and (5) in the paper [15]

2.3 Relay Phase

In this phase, R^* amplifies and forwards the received signal to S by using the harvested energy E_{R^*} in the duration of $(1-\alpha)T/2$. We ignore the processing power required by the transmit/receive the circuitry of R. The transmit power of R^* is given by

$$P_{R^*} = \frac{2\eta\alpha P_0 |h_r^*|^2}{(1-\alpha) d_{r^*}^{\theta}} = \frac{a P_0 |h_{r^*}|^2}{d_{r^*}^{\theta}}, \tag{4}$$

where $a = \frac{2\eta\alpha}{1-\alpha}$

Using the AF scheme, the transmit signal at R^* with transmit power P_{R^*} is given by

$$y_{R^*} = Gy_2, \tag{5}$$

where G is the relaying gain in the AF scheme applied at R. G is expressed as

$$G \triangleq \sqrt{\frac{P_{R^*}}{P_1|h_3|^2/d_3^\theta + P_2|h_4|^2/d_4^\theta + \sigma^2}}. \tag{6}$$

The received signal at S in this phase is written as

$$y_3 = \frac{Gh_{r^*}}{\sqrt{d_{r^*}^\theta}}\left(\sqrt{\frac{P_1}{d_3^\theta}}h_3 s_1 + \sqrt{\frac{P_2}{d_4^\theta}}h_4 s_2 + n_2\right) + n_3, \tag{7}$$

where $n_3 \sim \mathcal{CN}(0, \sigma^2)$

Assuming that S only uses the relaying signal to detect s_1 and s_2 by applying SIC, the instantaneous SINR to detect s_1 at S in this phase is expressed as

$$\begin{aligned}\gamma_r^{s_1} &= \frac{P_1 G^2 |h_3|^2 |h_{r^*}|^2 / d_3^\theta d_{r^*}\theta}{G^2(P_2|h_4|^2/d_4^\theta + \sigma^2)|h_{r^*}|^2/d_{r^*}^\theta + \sigma^2} \\ &= \frac{a\gamma_3\gamma_{r^*}|h_3|^2|h_{r^*}|^4}{\gamma_3|h_3|^2 + (\gamma_4|h_4|^2+1)(a\gamma_{r^*}|h_{r^*}|^4+1)}.\end{aligned} \tag{8}$$

The instantaneous SNR to detect s_2 at S in this phase is obtained by

$$\gamma_r^{s_2} = \frac{a\gamma_4\gamma_{r^*}|h_3|^2|h_{r^*}|^4}{\gamma_3|h_3|^2 + \gamma_4|h_4|^2 + a\gamma_{r^*}|h_{r^*}|^4 + 1} \tag{9}$$

where $\gamma_{r^*} = \frac{P_0}{\sigma^2 d_{r^*}^\theta}, \gamma_3 = \frac{P_1}{\sigma^2 d_3^\theta}, \gamma_4 = \frac{P_2}{\sigma^2 d_4^\theta}$ are denoted as transmit SNR at S, U_1 and U_2, respectively.

By applying the SC scheme at S, the instantaneous SINR and SNR to detect s_1 and s_2 at S in this phase are respectively given by

$$\gamma_{s_1} = max\left\{\gamma_r^{s_1}, \gamma_d^{s_1}\right\}, \tag{10}$$

$$\gamma_{s_2} = max\left\{\gamma_r^{s_2}, \gamma_d^{s_2}\right\}. \tag{11}$$

Notice that $|h_i|^2$ ($i \in \{1, 2, 3, 4\}$) are assumed as the i.i.d. Rayleigh channel gains following exponential distributions with parameters λ_i Thus, the probability density function (PDF) and the cumulative distribution function (CDF) of these random variables $|h_i|^2$ are written as

$$f_{|h_i|^2}(x) = \frac{1}{\lambda_i}e^{-\frac{x}{\lambda_i}}, \tag{12}$$

$$F_{|h_i|^2}(x) = 1 - e^{-\frac{x}{\lambda_i}}. \tag{13}$$

R^* is the best capable of receiving power, selected from N relays. Therefore, PDF and CDF of the random variables $|h_{r^*}|^2$ are written as

$$f_{|h_{r^*}|^2}(x) = \frac{N}{\lambda_{r^*}} e^{-\frac{x}{\lambda_{r^*}}} \left(1 - e^{-\frac{x}{\lambda_{r^*}}}\right)^{(N-1)}, \tag{14}$$

$$F_{|h_{r^*}|^2}(x) = \left(1 - e^{-\frac{x}{\lambda_{r^*}}}\right)^N = \sum_{k=0}^{N} C_k^N (-1)^{N-k} e^{-\frac{(N-k)x}{\lambda_{r^*}}}. \tag{15}$$

For further calculation, first we derive the expressions of CDF and PDF of $X = \frac{\gamma_j |h_j|^2}{\gamma_k |h_k|^2 + 1}$ as follows

$$F_X(x) = \Pr\left(\frac{\gamma_j |h_j|^2}{\gamma_k |h_k|^2 + 1} < x\right) = 1 - \frac{\lambda_j \gamma_j e^{-\frac{x}{\lambda_j \gamma_j}}}{\lambda_j \gamma_j + \lambda_k \gamma_k x}. \tag{16}$$

$$f_X(x) = \frac{\lambda_j \gamma_j \lambda_k \gamma_k e^{-\frac{x}{\lambda_j \gamma_j}}}{(\lambda_j \gamma_j + \lambda_k \gamma_k x)^2} + \frac{e^{-\frac{x}{\lambda_j \gamma_j}}}{\lambda_j \gamma_j + \lambda_k \gamma_k x}. \tag{17}$$

where $j \in \{1, 3\}, k \in \{2, 4\}$

3 Performance Analysis

In this section, we analyze the performance of this considered system in terms of outage probability (P_{out}) and throughput (τ). The outage probability P_{out} is defined as the probability that the instantaneous capacity,

$$C = \frac{1 - \alpha}{2} log_2(1 + SINR). \tag{18}$$

falls below a predetermined rate threshold. We assume that $R_{th} > 0(bps/Hz)$ is the minimum required data rate for both users. Therefore, P_{out} is expressed as follows

$$\begin{aligned} P_{out} &= Pr\left(\frac{1 - \alpha}{2} log_2(1 + SINR) < R_{th}\right) \\ &= Pr\left(SINR < 2^{\frac{2R_{th}}{1-\alpha}} - 1 \triangleq \gamma_{th}\right). \end{aligned} \tag{19}$$

For our considered system, the outage probability $P_{out}^{s_1}$ for detecting s_1 and $P_{out}^{s_2}$ for detecting s_2 are expressed as

$$P_{out}^{s_1} = Pr(\gamma_{s_1} < \gamma_{th}) = Pr(\gamma_d^{s_1} < \gamma_{th}) \cdot Pr(\gamma_r^{s_1} < \gamma_{th}), \tag{20}$$

$$P_{out}^{s_2} = Pr(\gamma_{s_2} < \gamma_{th}) = Pr(\gamma_d^{s_2} < \gamma_{th}) \cdot Pr(\gamma_r^{s_2} < \gamma_{th}), \tag{21}$$

respectively.

Proposition 1. *Under Rayleigh fading, the outage probability $P_{out}^{s_1}$ for detecting s_1 for detecting is given by (22) and (23), respectively.*

$$Pr(\gamma_d^{s_1} < \gamma_{th}) = 1 - \frac{\gamma_1\lambda_1}{\gamma_{th}\gamma_2\lambda_2 + \gamma_1\lambda_1} e^{-\frac{\gamma_t}{\gamma_1\lambda_1}} \tag{22}$$

$$Pr(\gamma_r^{s1} < \gamma_{th}) = 1 - \frac{(-1)^N \pi\mu e^{-\frac{\gamma_{th}}{\lambda_3\gamma_3}}}{M} \sum_{k=1}^{N} C_k^N (-1)^{(N-k)} \sum_{i=1}^{M} u_i \sqrt[k]{\left(\frac{\mu}{ln^2 u_i} + \gamma_{th} + 1\right)} - 1 \times \frac{\lambda_3\gamma_3\lambda_4\gamma_4 + \lambda_3\gamma_3 + \lambda_4\gamma_4(\frac{\mu}{ln^2 u_i} + \gamma_{th})}{\left[\lambda_3\gamma_3 + \lambda_4\gamma_4(\frac{\mu}{ln^2 u_i} + \gamma_{th})\right]^2 ln^3 u_i} e^{\frac{-\mu}{\lambda_3\gamma_3 ln^2 u_i}} \sqrt{1-\beta_i^2} \tag{23}$$

where $u_i = \frac{\beta_i+1}{2}$ with $\beta_i = \cos\left(\frac{2i-1}{2M}\pi\right)$, and M is the complexity-vs-accuracy trade-off coefficient.

Proof. See Appendix B.

Proposition 2. *Under Rayleigh fading, the outage probability $P_{out}^{s_2}$ for detecting s_2 is given by (24), respectively.*

$$P_{out}^{s2} = \left(1 - e^{-\frac{\gamma_{th}}{\lambda_2\gamma_2}}\right) \left[1 + \frac{\pi^2\mu e^{-\frac{\gamma_{th}}{\lambda_4\gamma_4}}}{2MH\lambda_4\gamma_4} \sum_{k=0}^{N} C_k^N (-1)^{N-k} \sum_{i=1}^{M}\sum_{j=1}^{H} e^{-\frac{\mu}{\lambda_4\gamma_4 ln^2 u_i}} \times \frac{u_i \sqrt[N-k]{\left(\frac{\mu}{ln^2 u_i} - \lambda_3\gamma_3 ln v_j + \gamma_{th} + 1\right)}}{u_i ln^3 u_i} \sqrt{(1-\phi_i^2)(1-\varphi_j^2)}\right] \tag{24}$$

where $u_i = \frac{\phi_i+1}{2}, \phi_i = cos(\frac{2i-1}{2M}\pi), v_j = \frac{\varphi_j+1}{2}, \varphi_j = cos(\frac{2j-1}{2H}\pi), M$ and H are the complexity-vs-accuracy trade-off coefficients.

Proof. See Appendix A.

Proposition 3. *The throughput expressions for U_1 and U_2 are respectively given by*

$$\tau_1 = \frac{R_{th}(1-\alpha)(1-P_{out}^{s_1})}{2}, \tag{25}$$

$$\tau_2 = \frac{R_{th}(1-\alpha)(1-P_{out}^{s_2})}{2}. \tag{26}$$

4 Nummerical Results and Disscussion

In this section, the performance of the system is analyzed based on the results of the outage probability and throughput of the system by using Monte-Carlo simulation.

No	Description	Notation	Value	Unit
1	The distances from S to U_1	d_1	3	
2	The distances from S to U_2	d_2	6	
3	The distances from R^* to U_1	d_3	2	
4	The distances from R^* to U_2	d_4	5	
5	The distances from S to R^*	d_{r^*}	1	
6	The rate threshold	R_{th}	1	bps/Hz
7	The variance of additive noises	σ^2	1	
8	The path loss exponent	θ	2	
9	The complexity-vs-accuracy trade-off coefficients	M, H	100	

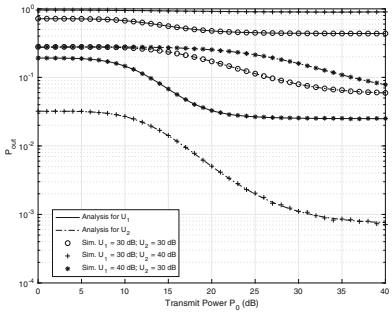

Fig. 2. Outage probability of the U_1 and U_2 versus P_0 with different values of (P_1, P_2) where $\alpha = 0.4, \eta = 0.8$

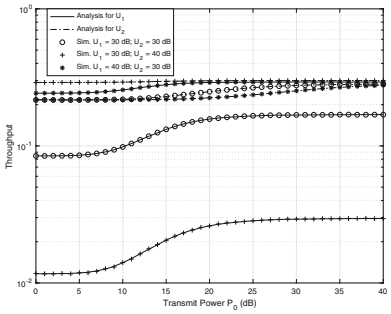

Fig. 3. Throughput of the U_1 and U_2 versus P_0 with different values of (P_1, P_2) where $\alpha = 0.4, \eta = 0.8$

The predefined simulation parameters are set in the table below:

Figure 2 and Fig. 3 show the system performance results, which are, particularly, the outage probability and the throughput at users U_1 and U_2, in comparison with transmit power at the base station (P_0) with different values of the transmit powers at users U_1 (P_1) and U_2 (P_2). Specifically, from Fig. 2, we can see that the outage probability at U_1 and U_2 decreases when increasing P_0. At the same time, when P_2 increases, the user's performance reduces as a result because of the increase in interference. This is explained in formulas (2) and (8). Similar conclusions are also obtained in case of considering the out probability for user U_2 in Fig. 2. Specifically, the system performance at user U_2 improves if we increase P_2 and decrease P_1, as shown in formulas (3) and (9). In Fig. 3, the throughputs of both users U_1 and U_2 improve when increasing P_0. In this result, we also see that, when increasing P_1 and decreasing P_2, the throughput of U_1 increases, in contrast, the throughput of U_2 increases when increasing P_2 and decreasing P_1.

The number of relay nodes is also an important parameter of the system. Figure 4 and Fig. 5 show the effect of the number of relays on the performance

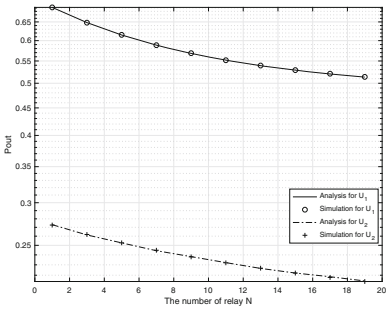

Fig. 4. Outage probability of the U_1 and U_2 versus the number of relays N; $P_0 = 15$ dB, $P_1 = 30$ dB, $P_2 = 30$ dB, $\alpha = 0.4, \eta = 0.8$

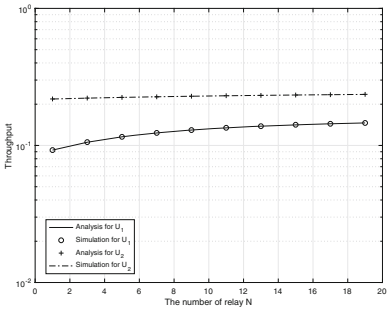

Fig. 5. Throughput of the U_1 and U_2 versus the number of relays N; $P_0 = 15$ dB, $P_1 = 30$ dB, $P_2 = 30$ dB, $\alpha = 0.4, \eta = 0.8$

of the system in terms of outage probability and throughput. In Fig. 4, the outage probability of both users decreases when increasing the number of relays. On the contrary, the throughput of both users increases in Fig. 5 when the number of relays increases. Through the above two results, we conclude that the performance of the system is improved when increasing the number of relays.

Figure 6 is the simulation result of the outage probability of both users U_1 and U_2 following the energy conversion efficiency. We see that the outage probability decreases with the increasing of the energy conversion efficiency. It means that the performance of the system in terms of the outage probability is improved by increasing this parameter. Figure 7 shows that the throughputs of both users U_1 and U_2 increases with an increase in energy conversion efficiency. The reason for the two results in Fig. 6 and Fig. 7 is that as the energy conversion efficiency increases, the energy for amplifying and forwarding at R^* increases, thus the signal transfer efficiency at the uplink of the system is increased.

The impact of time switching ratio on system performance in terms of outage probability is illustrated in Fig. 8. This result shows that, with the simulation parameters described on the table and the values: $P_0 = 15$ dB, $P_1 = 30$ dB, $P_2 = 30$ dB, $\eta = 0.8$, when increasing α ($\alpha > 0$) until 0.1, the outage probability of both users U_1 and U_2 decreases. Then, with the value of α ($\alpha > 0.1$) progressing to 1, the outage probability of both users U_1 and U_2 increases. Thereby, we find that there are a value of the time switching ratio at which the average outage probability is minimum. The algorithm for finding values of the time switching ratio to minimize the outage probability of this system will continue to be studied in the future.

The System performance simulation results in terms of throughput versus α were performed in Fig. 9, which performed a throughput simulation of both users U_1 and U_2. It can be observed that the throughput is reduced when we increase the value of the tim switching ratio.

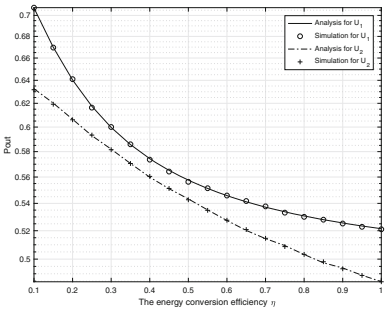

Fig. 6. Outage probability of the U_1 and U_2 versus the energy conversion efficiency; $P_0 = 15$ dB, $P_1 = 30$ dB, $P_2 = 30$ dB, $\alpha = 0.4$

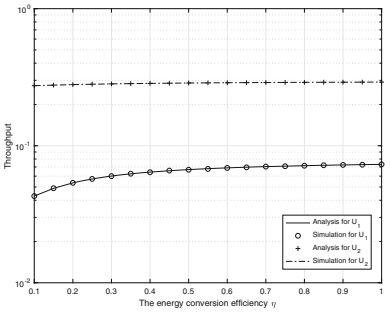

Fig. 7. Throughput of the U_1 and U_2 versus the energy conversion efficiency; $P_0 = 15$ dB, $P_1 = 30$ dB, $P_2 = 30$ dB, $\alpha = 0.4$

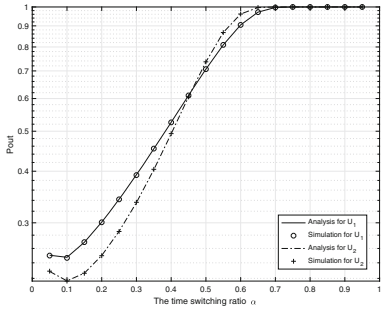

Fig. 8. Outage probability of the U_1 and U_2 versus the time switching ratio; where $P_0 = 15$ dB, $P_1 = 30$ dB, $P_2 = 30$ dB, $\eta = 0.8$

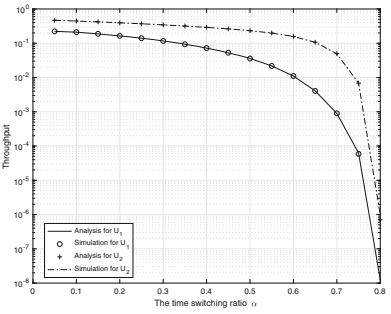

Fig. 9. Throughtput of the U_1 and U_2 versus the time switching ratio; where $P_0 = 15$ dB, $P_1 = 30$ dB, $P_2 = 30$ dB, $\eta = 0.8$

5 Conclusion

In this work, we studied an uplink cooperative NOMA network with wireless power transfer, in which, the best relay (i.e., the relay with the highest power received from the base station) helps the users forward information to the base station. The closed-form expressions of the outage probability and throughput for two users are given to describe the performance of the system. The simulation results showed that the performance of the U_1 can be improved when increasing P_0, P_1, N, and η. On the contrary, the performance of the U_1 decreases when increasing P_2. Similarly, the performance of the U_2 improves when increasing P_0, P_2, N, η and decreasing P_1. Especially, iteratively using numerical methods, we discovered that the system exists a value of time switching ratio that makes the average outage probability to be minimized. Therefore, we need to carefully consider the time switching ratio for the best system performance.

Appendix A

$$
\begin{aligned}
P_{out}^{s2} &= \Pr\left(\gamma_2|h_2|^2 < \gamma_{th}\right).\Pr\left(\frac{a\gamma_r\gamma_4|h_4|^2|h_{r^*}|^4}{a\gamma_{r^*}|h_{r^*}|^4+\gamma_3|h_3|^2+\gamma_4|h_4|^2+1} < \gamma_{th}\right) \\
&= F_{|h_2|^2}\left(\frac{\gamma_{th}}{\gamma_2}\right)\left[F_{|h_4|^2}\left(\frac{\gamma_{th}}{\gamma_4}\right)+\int_0^\infty\int_{\frac{\gamma_{th}}{\gamma_4}}^\infty F_{|h_{r^*}|^2}\right. \\
&\quad \left.\left(\sqrt{\frac{\gamma_{th}(\gamma_3 x+\gamma_4 y+1)}{a\gamma_{r^*}(\gamma_4 y-\gamma_{th})}}\right) f_{|h_4|^2}(y)dy f_{|h_3|^2}(x)dx\right] \\
&\overset{(a)}{=} \left(1-e^{-\frac{\gamma_{th}}{\lambda_2\gamma_2}}\right)\left[1+\frac{2\mu e^{-\frac{\gamma_{th}}{\lambda_4\gamma_4}}}{\lambda_3\lambda_4\gamma_4}\sum_{k=0}^{N}C_k^N(-1)^{N-k}\right. \\
&\quad \left.\int_0^\infty\int_0^1 \frac{z^{\sqrt[N-k]{\left(\gamma_3 x+\frac{\mu}{ln^2 z}+\gamma_{th}+1\right)}}.e^{-\frac{\mu}{\lambda_4\gamma_4 ln^2 z}-\frac{x}{\lambda_3}}}{z ln^3 z}dzdx\right] \\
&\overset{(b)}{=} \left(1-e^{-\frac{\gamma_{th}}{\lambda_2\gamma_2}}\right)\left[1+\frac{2\mu e^{-\frac{\gamma_{th}}{\lambda_4\gamma_4}}}{\lambda_3\lambda_4\gamma_4}\sum_{k=0}^{N}C_k^N(-1)^{N-k}\right. \\
&\quad \left.\times\int_0^\infty\frac{\pi}{2M}\sum_{i=1}^{M}\frac{u_i^{\sqrt[N-k]{\left(\gamma_3 x+\frac{\mu}{ln^2 u_i}+\gamma_{th}+1\right)}}.e^{-\frac{\mu}{\lambda_4\gamma_4 ln^2 u_i}-\frac{x}{\lambda_3}}\sqrt{1-\phi_i^2}}{u_i ln^3 u_i}dx\right] \\
&= \left(1-e^{-\frac{\gamma_{th}}{\lambda_2\gamma_2}}\right)\left[1+\frac{\pi\mu e^{-\frac{\gamma_{th}}{\lambda_4\gamma_4}}}{M\lambda_3\lambda_4\gamma_4}\sum_{k=0}^{N}C_k^N(-1)^{N-k}\sum_{i=1}^{M}\frac{e^{-\frac{\mu}{\lambda_4\gamma_4 ln^2 u_i}}\sqrt{1-\phi_i^2}}{u_i ln^3 u_i}\right. \\
&\quad \left.\times\int_0^\infty u_i^{\sqrt[N-k]{\left(\gamma_3 x+\frac{\mu}{ln^2 u_i}+\gamma_{th}+1\right)}}.e^{-\frac{x}{\lambda_3}}dx\right] \\
&\overset{(c)}{=} \left(1-e^{-\frac{\gamma_{th}}{\lambda_2\gamma_2}}\right)\left[1+\frac{\pi^2\mu e^{-\frac{\gamma_{th}}{\lambda_4\gamma_4}}}{2MH\lambda_4\gamma_4}\sum_{k=0}^{N}C_k^N(-1)^{N-k}\right. \\
&\quad \left.\times\sum_{i=1}^{M}\sum_{j=1}^{H}\frac{e^{-\frac{\mu}{\lambda_4\gamma_4 ln^2 u_i}}u_i^{\sqrt[N-k]{\left(\frac{\mu}{ln^2 u_i}-\lambda_3\gamma_3 ln v_j+\gamma_{th}+1\right)}}}{u_i ln^3 u_i}\sqrt{(1-\phi_i^2)(1-\varphi_j^2)}\right]
\end{aligned}
$$

where step (a) is obtained by letting $z = e^{-\sqrt{\frac{\mu}{(\gamma_4 y-\gamma_{th})}}}$ in which $\mu = \frac{\gamma_{th}}{a\lambda_{r^*}\gamma_{r^*}}$, step (b) and (c) are obtained by applying the Gaussian-Chebyshev quadrature method in which $u_i = \frac{\phi_i+1}{2}, \phi_i = cos(\frac{2i-1}{2M}\pi), v_j = \frac{\varphi_j+1}{2}, \varphi_j = cos(\frac{2j-1}{2H}\pi), M$ and H are the complexity-vs-accuracy trade-off coefficients.

Appendix B

$$
\begin{aligned}
Pr(\gamma_d^{s1} < \gamma_{th}) &= Pr\left(\frac{\gamma_1|h_1|^2}{\gamma_2|h_2|^2+1} < \gamma_{th}\right) = Pr\left(|h_1|^2 < \frac{\gamma_{th}(\gamma_2|h_2|^2+1)}{\gamma_1}\right) \\
&= \int_0^\infty F_{|h_1|^2}\left(\frac{\gamma_{th}(\gamma_2 x+1)}{\gamma_1}\right) f_{|h_2|^2}(x)dx \\
&= 1 - \frac{1}{\lambda_2}e^{-\frac{\gamma_{th}}{\lambda_1\gamma_1}}\int_0^\infty e^{-x\frac{\gamma_{th}\gamma_2\lambda_2+\gamma_1\lambda_1}{\gamma_1\lambda_1\lambda_2}}dx = 1 - \frac{\gamma_1\lambda_1}{\gamma_{th}\gamma_2\lambda_2+\gamma_1\lambda_1}e^{-\frac{\gamma_t}{\gamma_1\lambda_1}} \\
Pr(\gamma_r^{s1} < \gamma_{th}) &= \Pr\left(\frac{a\gamma_3\gamma_r|h_3|^2|h_{r^*}|^4}{(\gamma_4|h_4|^2+1)a\gamma_{r^*}|h_{r^*}|^4+\gamma_3|h_3|^2+\gamma_4|h_4|^2+1} < \gamma_{th}\right) \\
&= \Pr\left(a\gamma_r|h_{r^*}|^4\left[\gamma_3|h_3|^2-\gamma_{th}\left(\gamma_4|h_4|^2+1\right)\right] < \gamma_{th}\left[\gamma_3|h_3|^2+\gamma_4|h_4|^2+1\right]\right) \\
&= \Pr\left(\gamma_3|h_3|^2-\gamma_{th}(\gamma_4|h_4|^2+1) < 0\right) \\
&+ \Pr\left(|h_{r^*}|^4 < \frac{\gamma_{th}(\gamma_3|h_3|^2+\gamma_4|h_4|^2+1)}{a\gamma_{r^*}\left[\gamma_3|h_3|^2-\gamma_{th}(\gamma_4|h_4|^2+1)\right]}, \gamma_3|h_3|^2-\gamma_{th}(\gamma_4|h_4|^2+1) > 0\right) \\
&= \Pr\left(\frac{\gamma_3|h_3|^2}{\gamma_4|h_4|^2+1} < \gamma_{th}\right) + \Pr\left(|h_{r^*}|^4 < \frac{\gamma_{th}\left(\frac{\gamma_3|h_3|^2}{\gamma_4|h_4|^2+1}\right)}{a\gamma_{r^*}\left(\frac{\gamma_3|h_3|^2}{\gamma_4|h_4|^2+1}-\gamma_{th}\right)},\right. \\
&\left.\frac{\gamma_3|h_3|^2}{\gamma_4|h_4|^2+1} > \gamma_{th}\right) \\
&\overset{(a)}{=} 1+(-1)^N\sum_{k=1}^{N}C_k^N(-1)^{(N-k)}\int_0^\infty e^{-\frac{k}{\lambda_{r^*}}\sqrt{\frac{\gamma_{th}(y+\gamma_{th}+1)}{a\gamma_{th}y}}} \\
&\times\left[\frac{\lambda_3\gamma_3\lambda_4\gamma_4 e^{-\frac{y+\gamma_{th}}{\lambda_3\gamma_3}}}{(\lambda_3\gamma_3+\lambda_4\gamma_4(y+\gamma_{th}))^2}+\frac{e^{-\frac{y+\gamma_{th}}{\lambda_3\gamma_3}}}{(\lambda_3\gamma_3+\lambda_4\gamma_4(y+\gamma_{th}))}\right]dy \\
&\overset{(b)}{=} 1+2(-1)^N\mu e^{-\frac{\gamma_{th}}{\lambda_3\gamma_3}}\sum_{k=1}^{N}C_k^N(-1)^{(N-k)}\int_0^1 z^{\sqrt[k]{\left(\frac{\mu}{ln^2 z}+\gamma_{th}+1\right)}-1} \\
&\times\frac{\lambda_3\gamma_3\lambda_4\gamma_4+\lambda_3\gamma_3\lambda_4\gamma_4\left(\frac{\mu}{ln^2 z}+\gamma_{th}\right)}{\left[\lambda_3\gamma_3+\lambda_4\gamma_4\left(\frac{\mu}{ln^2 z}+\gamma_{th}\right)\right]^2 ln^3 z}e^{-\frac{\mu}{\lambda_3\gamma_3 ln^2 z}}dz \\
&\overset{(c)}{=} 1-\frac{(-1)^N\pi\mu e^{-\frac{\gamma_{th}}{\lambda_3\gamma_3}}}{M}\sum_{k=1}^{N}C_k^N(-1)^{(N-k)}\sum_{i=1}^{M}u_i\sqrt[k]{\left(\frac{\mu}{ln^2 u_i}+\gamma_{th}+1\right)}-1 \\
&\times\frac{\lambda_3\gamma_3\lambda_4\gamma_4+\lambda_3\gamma_3+\lambda_4\gamma_4(\frac{\mu}{ln^2 u_i}+\gamma_{th})}{\left[\lambda_3\gamma_3+\lambda_4\gamma_4(\frac{\mu}{ln^2 u_i}+\gamma_{th})\right]^2 ln^3 u_i}e^{\frac{-\mu}{\lambda_3\gamma_3 ln^2 u_i}}\sqrt{1-\beta_i^2}
\end{aligned}
$$

where step (a) is obtained by using Eqs. (13) and (17), step (b) is obtained by letting $z = e^{-\frac{\mu}{\sqrt{y}}}$ in which $\mu = \frac{\gamma_{th}}{a\lambda_{r^*}^2\gamma_{r^*}}$, step (c) is obtained by applying the Gaussian-Chebyshev quadrature method in which $u_i = \frac{\beta_i+1}{2}$ with $\beta_i = \cos\left(\frac{2i-1}{2M}\pi\right)$, and M is the complexity-vs-accuracy trade-off coefficient.

References

1. Zhang, J.W., Bai, X., Han, W.Y., Zhao, B.H., Xu, L.J., Wei, J.J.: The design of radio frequency energy harvesting and radio frequency-based wireless power transfer system for battery-less self-sustaining applications. Int. J. RF Microwave Comput. Aided Eng. **29**(1), e21658 (2019)

2. Lu, X., Wang, P., Niyato, D., Kim, D.I., Han, Z.: Wireless networks with RF energy harvesting: a contemporary survey. IEEE Commun. Surv. Tutorial **17**(2), 757–789 (2014)
3. Ha, D.B., Agrawal, J.P.: Performance analysis for NOMA relaying system in next-generation networks with RF energy harvesting. In: Wireless Energy Transfer Technology. IntechOpen (2019)
4. Huang, K., Lau, V.K.: Enabling wireless power transfer in cellular networks: architecture, modeling and deployment. IEEE Trans. Wireless Commun. **13**(2), 902–912 (2019)
5. Divakaran, S.K., Krishna, D.D.: RF energy harvesting systems: an overview and design issues. Int. J. RF Microwave Comput. Aided Eng. **29**(1), e21633 (2019)
6. Tabassum, H., Ali, M.S., Hossain, E., Hossain, M., Kim, D.I.: Non-orthogonal multiple access (NOMA) in cellular uplink and downlink: challenges and enabling techniques. arXiv preprint arXiv:1608.05783 (2016)
7. Zaidi, S.K., Hasan, S.F., Gui, X.: Evaluating the ergodic rate in SWIPT-aided hybrid NOMA. IEEE Commun. Lett. **22**(9), 1870–1873 (2018)
8. Liu, Y., Ding, Z., Elkashlan, M., Poor, H.V.: Cooperative non-orthogonal multiple access with simultaneous wireless information and power transfer. IEEE J. Sel. Areas Commun. **34**(4), 938–953 (2016)
9. Zhu, J., Wang, J., Huang, Y., Navaie, K., Ding, Z., Yang, L.: On optimal beamforming design for downlink MISO NOMA systems. IEEE Trans. Veh. Technol. **69**, 3008–3020 (2020)
10. Wang, L., Xu, D.: Resource allocation in downlink SWIPT-based cooperative NOMA systems. KSII Trans. Internet Inf. Syst. **14**(1), 20–39 (2020)
11. Kim, J.O., Uddin, M.B., Shin, S.Y.: Outage analysis of NOMA exploited coordinated direct and relay assisted uplink transmission. In: Proceedings of the 7th International Conference on Information and Communication Technology (ICoICT 2019), pp. 1–6. IEEE (2019)
12. Xu, Y., Wang, G., Li, B., Jia, S.: Performance of D2D aided uplink coordinated direct and relay transmission using NOMA. IEEE Access **7**, 151090–151102 (2019)
13. Nomikos, N., Michailidis, E.T., Trakadas, P., Vouyioukas, D., Zahariadis, T., Krikidis, I.: Flex-NOMA: exploiting buffer-aided relay selection for massive connectivity in the 5G uplink. IEEE Access **7**, 88743–88755 (2019)
14. Yue, X., Liu, Y., Kang, S., Nallanathan, A., Ding, Z.: Exploiting full/half-duplex user relaying in NOMA systems. IEEE Trans. Commun. **66**(2), 560–575 (2017)
15. HA, B.D., Tran, D.D., Vo, S.N.: Cooperative transmission in uplink NOMA networks with wireless power transfer. J. Sci. Technol. Issue Inf. Commun. Technol. **17**(122), 20–27 (2019)